Anion-exchange synthesis of hollow $BiOCl/Bi_2S_3$ hybrids with superior capability for photocatalytic reduction of hexavalent chromium under visible light irradiation

Feifan Xu, Gang Cheng ✉, Yi Wei, Rong Chen

School of Chemistry and Environmental Engineering, Wuhan Institute of Technology, Xiongchu Avenue, Wuhan 430073, People's Republic of China
✉ *E-mail: gchenglab@163.com*

Published in Micro & Nano Letters; Received on 20th February 2017; Revised on 3rd May 2017; Accepted on 10th July 2017

$BiOCl/Bi_2S_3$ hollow hybrids were synthesised through a mild anion-exchange method from BiOCl microspheres and thiacetamide. X-ray diffraction, scanning electron microscopy, transmission electron microscopy, nitrogen adsorption measurements, ultraviolet–visible–near-infrared diffuse reflectance spectra, photocurrent, and electrochemical impedance spectroscopy (EIS) were employed to study the composition, structure, and properties of the as-synthesised $BiOCl/Bi_2S_3$ hybrids. Compared to pure Bi_2S_3 and BiOCl products, the as-prepared $BiOCl/Bi_2S_3$ hollow hybrids exhibited superior capability for photocatalytic reduction of hexavalent chromium under vis light irradiation. The photocurrent and EIS results demonstrated that the low recombination rate of photoinduced electron–hole pairs was contributed to the enhanced photoreduction activity.

1. Introduction: Hexavalent chromium [Cr(VI)] is a highly toxic contaminant and can cause health problem such as cancer, pulmonary congestions, and liver damage [1, 2]. Therefore, much effort has been made to develop efficient and economical technologies to eliminate Cr(VI) contamination in the past decades [3, 4]. Semiconductor-based photocatalysis is regarded as one of most attractive techniques for Cr(VI) removal via photocatalytic reduction of Cr(VI) to Cr(III), which shows relative low toxicity [5, 6]. To achieve this goal, it is significant to explore excellent semiconductors for constructing an efficient photocatalysis system. In general, single semiconductor-involved photocatalysis system suffered from the drawback of recombination of photoinduced electron–hole pairs [7, 8]. Accordingly, a semiconductor–semiconductor composited photocatalysis system possessing enhanced charge separation and interfacial charge-transfer efficiency has been one of the major concerns in contaminants removal over the past decades [9–11].

In recent years, Bismuth Oxychloride (BiOCl) semiconductor has been widely used as the photocatalyst for pollutants removal due to its unique optical and electrical properties [12–14]. However, most of the studies focused on the photocatalytic degradation of organic contaminants, and there are few reports relevant to photoreduction of Cr(VI) [15]. On the other hand, BiOCl has a wide bandgap and can only be excited by ultraviolet light, which extremely limits its practise application. Although coupling with another bismuth (Bi)-containing semiconductor such as Bismuth Molybdenum Oxide (Bi_2MoO_6) [16], bismuthyl iodide (BiOI) [17], and Bismuth Vanadate ($BiVO_4$) [18] has been attempted to broad the light absorption and improve the separation efficiency of photogenerated electrons and holes, it is an interesting topic to explore suitable Bi-based candidate for fabrication of highly efficient composited photocatalysis system to achieve the remediation of highly toxic Cr(VI) wastewater. Bismuth Sulfide (Bi_2S_3) is one of good candidates as it displays narrow bandgap, but most of the Bismuth Oxychloride/Bismuth Sulfide ($BiOCl/Bi_2S_3$) photocatalysts were employed to degrade organic pollutants such as rhodamine B and 2,4-dichlorophenol [19–21].

Herein, combining with the advantages of both BiOCl and Bi_2S_3, a novel hollow $BiOCl/Bi_2S_3$ hybrid was successfully synthesised by a mild anion-exchange method using thiacetamide (TAA) as an etching agent and BiOCl microspheres as Bi-precursor. The as-prepared hollow $BiOCl/Bi_2S_3$ hybrid was used as an efficient photocatalyst for Cr(VI) photoreduction under visible (vis) light irradiation. The improved photoreduction capability of the $BiOCl/Bi_2S_3$ hybrid was also discussed.

2. Experimental section: Sodium chlorate ($NaClO_3$), ethylene glycol (EG), and triethylene glycol (TEG) were provided by Sinopharm Chemical Reagent Co., Ltd. (China). Bismuth Nitrate Pentahydrate ($Bi(NO_3)_3{\cdot}5H_2O$), thiacetamide, Sodium sulfide nanohydrate ($Na_2S{\cdot}9H_2O$), and tetrabutyl titanate were purchased from Aladdin (Shanghai, China). All chemicals were of analytical grade and used directly without further purification. Deionised water was used throughout this Letter.

In a typical synthesis of pure Bi_2S_3, 1 mmol $Bi(NO_3)_3{\cdot}5H_2O$ was dispersed in 35 mL EG and then added into 2 mmol $Na_2S{\cdot}9H_2O$. After that, the mixture was put into in a 50 mL Teflon-lined autoclave and keep at 180°C for 6 h. The final products were collected and washed with ethanol five times.

BiOCl microspheres were synthesised according to the previous report with a minor modification [13]. In a typical synthesis, 1.455 g $Bi(NO_3)_3{\cdot}5H_2O$ (3 mmol) was put into a round-bottom flask which contained 75 ml TEG. The mixture was stirred and sonicated until $Bi(NO_3)_3{\cdot}5H_2O$ was dissolved, followed by the addition of 0.318 g $NaClO_3$ (3 mmol), resulting in the formation of homogeneous suspension. Then, the mixture was transferred to a teflon-lined stainless steel autoclave to perform solvothermal process at 150°C for 3 h. After cooling down to room temperature, the solid product was collected by centrifugation and washed with deionised water for five times to remove possible remaining impurity.

$BiOCl/Bi_2S_3$ hybrid was synthesised through an anion-exchange method. In a typical procedure, 0.26 g BiOCl was put into 20 ml deionised water and sonicated for 10 min, and then added into 20 ml of TAA (2.5 mmol) aqueous solution to get a homogeneous suspension. The resulting suspension was transferred into a 50 ml teflon-lined autoclave and then maintained at 150°C for 2 h. Finally, the products were collected and washed thoroughly with deionised water and ethanol five times. For comparison, pure Bi_2S_3 products were also prepared and the detail was presented in supporting information.

The composition and structure of the as-prepared products were characterised by powder X-ray diffraction (XRD, Bruker axs D8 Discover), scanning electron microscopy (SEM, Hitachi SU8000) and transmission electron microscopy (TEM, Philips Tecnai G2 20). Brunauer–Emmett–Teller (BET) specific surface area was

doi: 10.1049/mnl.2017.0092

analysed by nitrogen adsorption in a Micromeritics Accelerated Surface Area and Porosimetry System (ASAP) 2020 nitrogen adsorption apparatus (USA). Ultraviolet–vis–near-infrared (UV–vis–NIR) diffuse reflectance spectra (DRS) were recorded on a UV–vis spectrophotometer (Shimadzu UV-2550) equipped with an integrating sphere attachment. The photoelectrochemical measurements were performed on a CHI660E electrochemistry workstation (Shanghai, China) at room temperature.

In a typical Cr(VI) photoreduction experiment, a 500 W xenon lamp with a 400 nm cut-off filter was used as light source. In a typical test, 20 mg of photocatalyst was dispersed in 40 ml Cr(VI) solution (40 and 80 mg/l) and magnetically stirred in dark for 60 min to achieve an adsorption−desorption equilibrium of Cr(VI) solution. The solutions got at each irradiation time interval were analysed by a Shimadzu UV2800 spectrophotometer, and the characteristic absorption of dichromate ions at 350 nm was used to monitor the photoreduction process. In addition, the cycling experiments of $BiOCl/Bi_2S_3$ hollow hybrids for Cr(VI) reduction were carried out as follows: 20 mg of $BiOCl/Bi_2S_3$ sample was dispersed in 40 ml Cr(VI) solution and magnetically stirred in dark to achieve an adsorption−desorption equilibrium. At specific irradiation time interval, the suspension was collected and then centrifuged to get the supernatant liquid. Then, the supernatant liquid was analysed by a Shimadzu UV2800 spectrophotometer and finally the Cr(VI) photoreduction curve was drawn. The above whole process finished the first cycle experiment. Then, all the solid sample in the first cycle was collected and dried in oven at 60°C and finally used as the photocatalyst in the second cycle. The sampling and analysis process of Cr(VI) solution in the second cycle are same to the first cycle. Analogously, the circulating runs of the photocatalytic reduction of Cr(VI) solution were performed five times in the end.

All the experiments were carried out in a standard three-electrode cells containing 0.5 mol/l Sodium Sulfate (Na_2SO_4) aqueous solution with a platinum foil and a saturated calomel electrode as the counter electrode and the reference electrode [22]. The working electrode was prepared according to the following process: 20 mg of as-prepared sample was mixed with 1 ml of N, N-Dimethylformamide (DMF) and 0.01 ml of nafion solution (5%, DuPont) to form homogeneous ink. Then, 0.1 ml of the catalyst ink was dip coated on a 10 mm × 10 mm indium−tin oxide glass electrode. The estimated loading amount of the sample is 2 mg/cm^2. After drying in room temperature, the as-prepared electrode was further annealed at 150°C for 4 h in a vacuum oven to remove the resin. Photocurrent responses of the photocatalyst as light on and off were measured at open-circuit potential, with simulated light irradiation provided by a 50 W xenon lamp. Electrochemical impedance spectroscopy (EIS) was carried out at the open-circuit potential in 0.5 M potassium ferricyanide solution. Samples were dip coated into a glassy carbon working electrode. A sinusoidal AC perturbation of 5 mV was applied to the electrode over the frequency range 1–10^5 Hz.

3. Results and discussion: As shown in Fig. 1*a*, all the diffraction peaks are readily indexed to the tetragonal phase of BiOCl (JCPDS Card No. 6-249), indicating the high purity of BiOCl synthesised according to the previous method. The SEM (Fig. 1*b* and inset) and TEM image (Fig. 1*c*) show that the BiOCl products display a hierarchical microsphere structure with the diameter of ∼2 µm, which composed of many tiny nanosheets and a large number of pore channels.

When 1 mmol BiOCl and 2.5 mmol TAA (excess amount) were used as the precursors and hydrothermally treated for 2 h, the XRD pattern (Fig. 1*d*) revealed the final product was BiOCl/Bi_2S_3 hybrid instead of pure Bi_2S_3. It means an absolute transformation from BiOCl to Bi_2S_3 did not occur, which might be due to a rapid formation of Bi_2S_3 covered on the surface of BiOCl microsphere via an anion-exchange etching, preventing the thorough

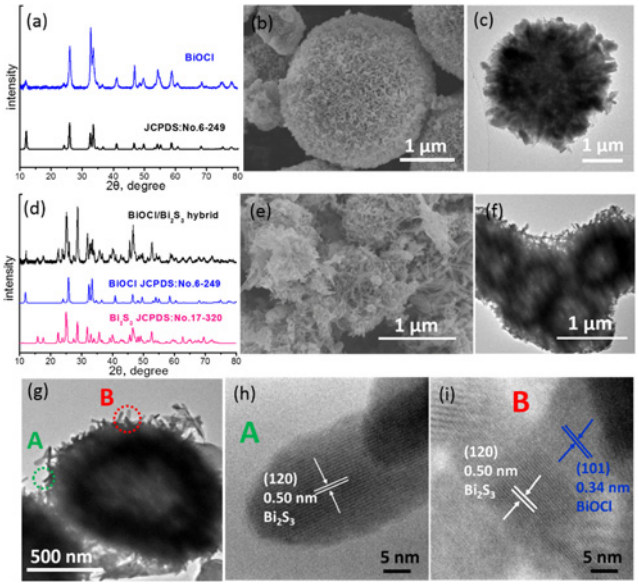

Fig. 1 *The characterisation of*
a XRD patterns
b SEM image and
c TEM image of the BiOCl samples
d XRD patterns
e SEM image
f, *g* TEM image and
h, *i* High-resolution TEM of the $BiOCl/Bi_2S_3$ products

transformation of BiOCl to Bi_2S_3 [23]. As can be seen in Fig. 1*e* and inset, the $BiOCl/Bi_2S_3$ hybrid still keeps the spherical structure, but it comprises of curved nanorods. However, the TEM images (Figs. 1*f* and *g*) indicate that the as-synthesised $BiOCl/Bi_2S_3$ hybrids were composed of aggregated hollow nanostructures. Each hollow microsphere has a diameter of about 1 µm and plenty of rod-like structures were embedded in the spherical hollow structure. As shown in Fig. 1*h*, a lattice fringe spacing with 0.50 nm corresponding to (120) plane of Bi_2S_3 was observed, indicated the formation of Bi_2S_3 on the surface of the microspheres, which might be attributed to the etching of TAA. Furthermore, as displayed in Fig. 1*i*, the lattice fringe spacing with 0.50 and 0.34 nm are agreement with (120) plane of Bi_2S_3 and (101) plane of BiOCl, respectively, further confirming the formation of $BiOCl/Bi_2S_3$ hybrids. On the basis of the above results, it is proposed that Bi_2S_3 crystal was first formed on the surface through the initial anion-exchange reaction between BiOCl and S^{2-} during the hydrothermal process. Subsequently, the outward diffusion rate of Bi^{3+} was faster than the inward diffusion rate of S^{2-}, resulting in the evacuation of Bi^{3+} in the inner region and formation of the hollow interior [10, 24].

As shown in Fig. 2*a*, the N_2 adsorption–desorption isotherm shows a typical type-IV isotherm with a hysteresis loop, which suggests that the $BiOCl/Bi_2S_3$ products contain abundant mesopores. The BET surface area of the hollow $BiOCl/Bi_2S_3$ hybrid was calculated to be 27.5 m^2/g. The Barrett−Joyner−Halenda pore size distribution curve as shown in Fig. 2*b* displays the average size of mesopores is about 28.6 nm. It is noted that the hollow $BiOCl/Bi_2S_3$ products with mesoporous structure are capable of boosting the light absorption and photochemical reactions even inside the interior region of the catalyst.

The Cr(VI) photoreduction capability of the as-synthesised pure Bi_2S_3 nanorod, BiOCl microsphere and $BiOCl/Bi_2S_3$ hybrid (SEM images were shown in on top of Fig. 3) were shown in Fig. 3*a*. It was found the as-prepared $BiOCl/Bi_2S_3$ hybrid exhibits higher photocatalytic activity toward 80 mg/l Cr(VI) solution compared with pure BiOCl and Bi_2S_3 samples, though the Cr(VI) solution

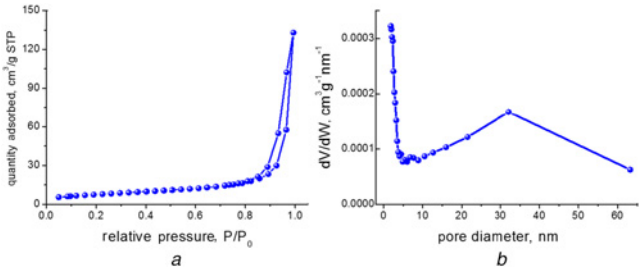

Fig. 2 *The characterisation by BET measurement*
a N_2 adsorption–desorption isotherm
b Pore size distribution of the hollow BiOCl/Bi_2S_3 hybrids

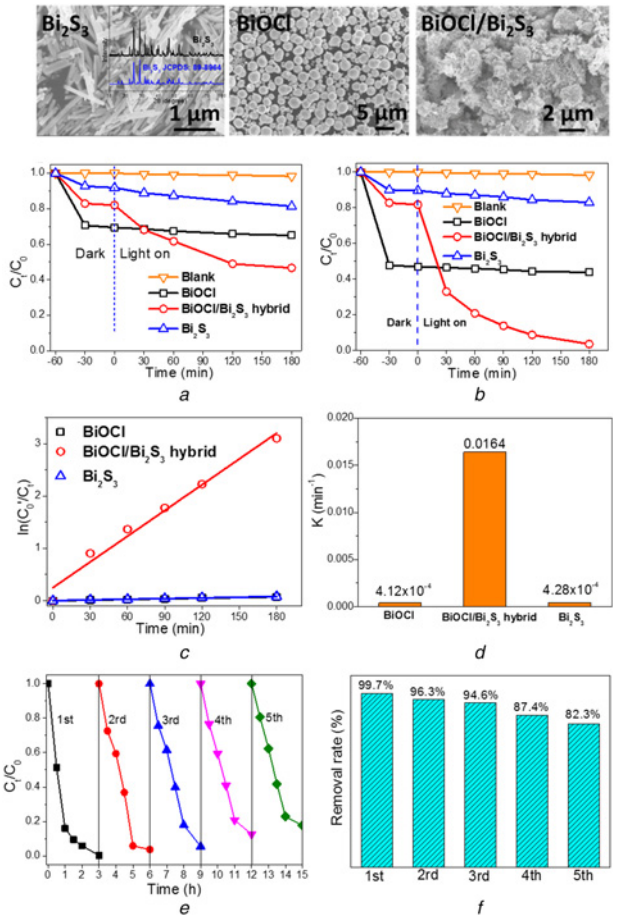

Fig. 3 *Photocatalytic reduction of*
a 80 mg/l Cr(VI)
b 40 mg/l Cr(VI)
c Reaction kinetics
d Rate constant *k* of the different samples
e Recycling performance of the BiOCl/Bi_2S_3 hybrids
f Corresponding removal rate of Cr(VI)solution

was not reduced completely. However, when the concentration of Cr(VI) solution was tuned to 40 mg/l, it was found the hollow BiOCl/Bi_2S_3 hybrid showed the superior photoreduction capability, and the Cr(VI) solution was almost completely removed within 180 min. The corresponding reaction kinetics was also discussed using the pseudo-first-order model, $\ln(C'_0/C_t)=kt$, where k is the rate constant (min^{-1}), C'_0 and C_t are the concentrations of Cr(VI) solution at initial time and t time in photocatalytic process. Fig. 3*c* describes the photoreduction reaction kinetics on the basis of data plotted in Fig. 3*b*. The determined reaction rates constant k was listed in Fig. 3*d*. It can be clearly seen that the rates constant of BiOCl/Bi_2S_3 hybrid was larger than pure BiOCl and Bi_2S_3,

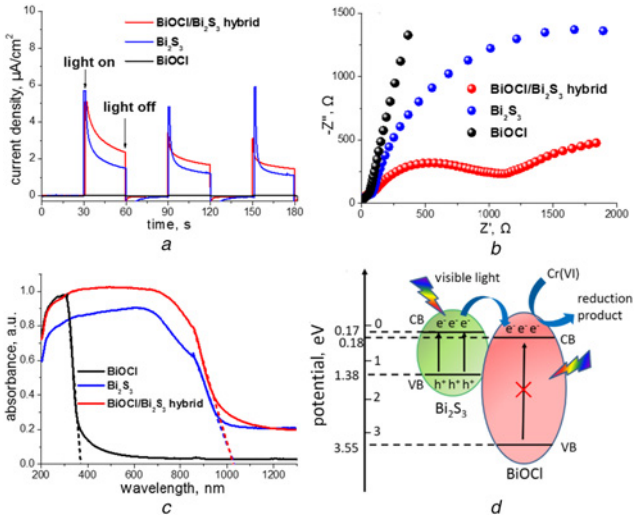

Fig. 4 *The enhanced photocatalytic mechanism characterisation of*
a Transient photocurrent density
b EIS Nyquist plots
c UV–VIS–NIR DRS spectra and
d Possible charge separation and transfer process of hollow BiOCl/Bi_2S_3 samples

which further confirms the remarkable photoreduction activity of such BiOCl/Bi_2S_3 hybrid. In addition, the recycling performance of the photocatalysts was a critical issue for long-term use in practical applications. As shown in Fig. 3*e*, the five cycling experiments were carried out and the photocatalytic activity of BiOCl/Bi_2S_3 hollow hybrids for Cr(VI) reduction was relatively stable though having a weak decreasing trend. It also can be observed that the removal rate of Cr(VI) solution after five cycles is still over 80% (Fig. 3*f*). The above results indicated that the BiOCl/Bi_2S_3 hollow hybrid was an efficient and relatively stable photocatalyst toward Cr(VI) removal.

Photocurrent response and EIS were widely used to investigate separation efficiency and charge-transfer capability of the photoinduced electron and holes in the photocatalyst during the photocatalysis reaction [22, 25]. As shown in Fig. 4*a*, there is almost no photocurrent on BiOCl regardless of whether there is light or not. However, the BiOCl/Bi_2S_3 hybrid showed a rapid and dramatic photocurrent generation during vis light illumination, revealing a higher separation efficiency of photoinduced electron–hole pairs in the BiOCl/Bi_2S_3 hybrid. As shown in the EIS spectra (Fig. 4*b*), the arc radius of BiOCl/Bi_2S_3 is much smaller than that of pure BiOCl and Bi_2S_3, demonstrating that the BiOCl/Bi_2S_3 hybrid has a positive effect on photoinduced carriers transfer [26, 27]. In other words, the higher photoreduction capability of the BiOCl/Bi_2S_3 hybrid was attributed to the higher separation efficiency of photogenerated carriers and lower recombination efficiency of photoinduced electron–hole pairs.

As a matter of fact, the bandgap of BiOCl and Bi_2S_3 could be calculated to be 3.37 and 1.21 eV, respectively, according to the UV–vis–NIR DRS (Fig. 4*c*). The positions of conduction and valence band can be calculated by the following equation [28, 29]:

$$E_{CB} = X - E_e - 0.5E_g \quad (1)$$

$$E_{VB} = E_{CB} + E_g \quad (2)$$

where E_{CB} is the conduction band (CB) edge potential. The X values for BiOCl and Bi_2S_3 are about 6.36 and 5.27 eV, respectively [21]. The E_e value is ~4.5 eV. The E_g values of BiOCl and Bi_2S_3 are 3.37 and 1.21 eV, respectively. The E_{CB} values are calculated at about 0.18 and 0.17 eV. Correspondingly, the Valence Band (VB) edge potentials (E_{VB}) are estimated to be about 3.55

doi: 10.1049/mnl.2017.0092

and 1.38 eV, respectively. On the basis of the above results, a possible pathway for Cr(VI) photocatalytic reduction was proposed. As shown in Fig. 4*d*, Bi_2S_3 would be excited on the vis light irradiation. Consequently, the excited electrons on the CB of Bi_2S_3 could migrate to the CB of BiOCl, which inhibits the recombination of photogenerated electron–hole pairs, resulting in more electrons to react with Cr(VI) adsorbed on the surface of BiOCl/Bi_2S_3 and final improvement of the photoreduction capability.

4. Conclusion: In summary, BiOCl/Bi_2S_3 hybrid with hollow nanostructure was successfully synthesised by a facile anion-exchange approach. Compared to pure BiOCl and Bi_2S_3, the BiOCl/Bi_2S_3 hybrid exhibited higher photocatalytic activity in reduction of Cr(VI) solution under vis light irradiation. The enhanced photoreduction capability of the BiOCl/Bi_2S_3 hybrid was attributed to separation of photoinduced electron−holes pairs and fast transfer ability of photogenerated charge carriers. It is expected that the as-prepared BiOCl/Bi_2S_3 composite materials could have great potential in Cr(VI) photoreduction removal.

5. Acknowledgments: This work was supported by the National Natural Science Foundation of China (grant no. 21501137) and the Department of Education of Hubei Province under the project of Science and Technology Innovation Team of Outstanding Young and Middle-aged Scientists (grant no. T201606).

6 References

[1] Mu R., Xu Z., Li L., *et al.*: 'On the photocatalytic properties of elongated TiO_2 nanoparticles for phenol degradation and Cr(VI) reduction', *J. Hazard. Mater.*, 2010, **176**, pp. 495–502

[2] Zhang Y.C., Li J., Zhang M., *et al.*: 'Size-tunable hydrothermal synthesis of SnS_2 nanocrystals with high performance in visible light-driven photocatalytic reduction of aqueous Cr(VI)', *Environ. Sci. Technol.*, 2011, **45**, pp. 9324–9331

[3] Weng B., Zhang X., Zhang N., *et al.*: 'Two-dimensional MoS_2 nanosheet-coated Bi_2S_3 discoids: synthesis, formation mechanism, and photocatalytic application', *Langmuir*, 2015, **31**, pp. 4314–4322

[4] Yang M.-Q., Zhang N., Wang Y., *et al.*: 'Metal-free, robust, and regenerable 3D graphene–organics aerogel with high and stable photosensitization efficiency', *J. Catal.*, 2017, **346**, pp. 21–29

[5] Yu J., Zhuang S., Xu X., *et al.*: 'Photogenerated electron reservoir in hetero-p-n CuO–ZnO nanocomposite device for visible-light-driven photocatalytic reduction of aqueous Cr(VI)', *J. Mater. Chem. A*, 2015, **3**, pp. 1199–1207

[6] Wang J., Li X., Li X., *et al.*: 'Mesoporous yolk-shell SnS_2–TiO_2 visible photocatalysts with enhanced activity and durability in Cr(VI) reduction', *Nanoscale*, 2013, **5**, pp. 1876–1881

[7] Liu M., Qiu X., Miyauchi M., *et al.*: 'Energy-level matching of Fe(III) ions grafted at surface and doped in bulk for efficient visible-light photocatalysts', *J. Am. Chem. Soc.*, 2013, **135**, pp. 10064–10072

[8] Zhang Z., Zhang L., Hedhili M.N., *et al.*: 'Plasmonic gold nanocrystals coupled with photonic crystal seamlessly on TiO_2 nanotube photoelectrodes for efficient visible light photoelectrochemical water splitting', *Nano Lett.*, 2013, **13**, pp. 14–20

[9] Zhang Z., Wang W., Wang L., *et al.*: 'Enhancement of visible-light photocatalysis by coupling with narrow-band-gap semiconductor: a case study on Bi_2S_3/Bi_2WO_6', *ACS Appl. Mater. Interfaces*, 2012, **4**, pp. 593–597

[10] Gao X., Wu H.B., Zheng L., *et al.*: 'Formation of mesoporous heterostructured $BiVO_4$/Bi_2S_3 hollow discoids with enhanced photoactivity', *Angew. Chem.*, 2014, **126**, pp. 6027–6031

[11] Zhang N., Yang M.-Q., Liu S., *et al.*: 'Waltzing with the versatile platform of graphene to synthesize composite photocatalysts', *Chem. Rev.*, 2015, **115**, pp. 10307–10377

[12] Zhao K., Zhang L., Wang J., *et al.*: 'Surface structure-dependent molecular oxygen activation of BiOCl single-crystalline nanosheets', *J. Am. Chem. Soc.*, 2013, **135**, pp. 15750–15753

[13] Xiong J., Cheng G., Qin F., *et al.*: 'Tunable BiOCl hierarchical nanostructures for high-efficient photocatalysis under visible light irradiation', *Chem. Eng. J.*, 2013, **220**, pp. 228–236

[14] Xiong J., Cheng G., Li G., *et al.*: 'Well-crystallized square-like 2D BiOCl nanoplates: mannitol-assisted hydrothermal synthesis and improved visible-light-driven photocatalytic performance', *RSC Adv.*, 2011, **1**, pp. 1542–1553

[15] Li H., Zhang L.: 'Oxygen vacancy induced selective silver deposition on the {001} facets of BiOCl single-crystalline nanosheets for enhanced Cr(vi) and sodium pentachlorophenate removal under visible light', *Nanoscale*, 2014, **6**, pp. 7805–7810

[16] Yue D., Chen D., Wang Z., *et al.*: 'Enhancement of visible photocatalytic performances of a Bi_2MoO_6–BiOCl nanocomposite with plate-on-plate heterojunction structure', *Phys. Chem. Chem. Phys.*, 2014, **16**, pp. 26314–26321

[17] Sun L., Xiang L., Zhao X., *et al.*: 'Enhanced visible-light photocatalytic activity of BiOI/BiOCl heterojunctions: key role of crystal facet combination', *ACS Catal.*, 2015, **5**, pp. 3540–3551

[18] He Z., Shi Y., Gao C., *et al.*: 'BiOCl/$BiVO_4$ p–n heterojunction with enhanced photocatalytic activity under visible-light irradiation', *J. Phys. Chem. C*, 2014, **118**, pp. 389–398

[19] Jiang S., Zhou K., Shi Y., *et al.*: 'In situ synthesis of hierarchical flower-like Bi_2S_3/BiOCl composite with enhanced visible light photocatalytic activity', *Appl. Surf. Sci.*, 2014, **290**, pp. 313–319

[20] Cao J., Xu B.Y., Lin H. L., *et al.*: 'Novel Bi_2S_3-sensitized BiOCl with highly visible light photocatalytic activity for the removal of rhodamine B', *Catal. Commun.*, 2012, **26**, pp. 204–208

[21] Cheng H.F., Huang B.B., Qin X.Y., *et al.*: 'A controlled anion exchange strategy to synthesize Bi_2S_3 nanocrystals/BiOCl hybrid architectures with efficient visible light photoactivity', *Chem. Commun.*, 2012, **48**, pp. 97–99

[22] Cheng G., Xu F., Stadler F.J., *et al.*: 'A facile and general synthesis strategy to doped TiO_2 nanoaggregates with a mesoporous structure and comparable property', *RSC Adv.*, 2015, **5**, pp. 64293–64298

[23] Liang N., Zai J., Xu M., *et al.*: 'Novel Bi_2S_3/$Bi_2O_2CO_3$ heterojunction photocatalysts with enhanced visible light responsive activity and wastewater treatment', *J. Mater. Chem. A*, 2014, **2**, pp. 4208–4216

[24] Park J., Zheng H., Jun Y.-W., *et al.*: 'Hetero-epitaxial anion exchange yields single-crystalline hollow nanoparticles', *J. Am. Chem. Soc.*, 2009, **131**, pp. 13943–13945

[25] Li H., Sun Y., Cai B., *et al.*: 'Hierarchically Z-scheme photocatalyst of Ag@AgCl decorated on $BiVO_4$ (0 4 0) with enhancing photoelectrochemical and photocatalytic performance', *Appl. Catal. B, Environ.*, 2015, **170–171**, pp. 206–214

[26] Huang Q., Tian S., Zeng D., *et al.*: 'Enhanced photocatalytic activity of chemically bonded TiO_2/Graphene composites based on the effective interfacial charge transfer through the C–Ti bond', *ACS Catal.*, 2013, **3**, pp. 1477–1485

[27] Dai Z., Qin F., Zhao H., *et al.*: 'Time-dependent evolution of the $Bi_{3.64}Mo_{0.36}O_{6.55}$/$Bi_2MoO_6$ heterostructure for enhanced photocatalytic activity via the interfacial hole migration', *Nanoscale*, 2015, **7**, pp. 11991–11999

[28] Tian J., Hao P., Wei N., *et al.*: '3D Bi_2MoO_6 nanosheet/TiO_2 nanobelt heterostructure: enhanced photocatalytic activities and photoelectochemistry performance', *ACS Catal.*, 2015, **5**, pp. 4530–4536

[29] Zhang L.J., Li S., Liu B.K., *et al.*: 'Highly efficient CdS/WO_3 photocatalysts: Z-scheme photocatalytic mechanism for their enhanced photocatalytic H_2 evolution under visible light', *ACS Catal.*, 2014, **4**, pp. 3724–3729